DOI: 10.1002/cctc.201200050

Catalytic NO Oxidation Pathways and Redox Cycles on Dispersed Oxides of Rhodium and Cobalt

Brian M. Weiss,[a, c] Nancy Artioli,[a, d] and Enrique Iglesia*[a, b]

The elementary steps and site requirements for the oxidation of NO on Rh and Co and the oxidation state of the catalysts were probed by isotopic tracers, chemisorption methods, and kinetic measurements of the effects of the pressures of NO, O_2, and NO_2 on turnover rates. On both catalysts, NO oxidation rates were first order in NO and O_2 and were inversely proportional to NO_2 pressure, as observed on Pt and PdO. These data implied that O_2 activation on an isolated vacancy (*) on the catalyst surfaces that were saturated with oxygen (O*) was the kinetically relevant step. Quasi-equilibrated NO–NO_2 interconversion steps established the coverage of * and O* and the chemical potential of oxygen during the catalysis. These chemical potentials set the oxidation state of Rh and Co clusters and were described by an O_2 virtual pressure, which was determined from the formalism of non-equilibrium thermodynamics. RhO_2 and Co_3O_4 were the phases that were present during NO oxidation, which had several consequences for catalysis. Turnover rates increased with increasing cluster size because the vacancies that were needed for O_2 activation were more abundant on large oxide clusters, which delocalized electrons better than small clusters. NO oxidation turnover rates on RhO_2 and Co_3O_4 were higher than expected from the oxygen-binding energy on Rh and Co metal surfaces and from the reduction potentials of Rh^{3+} and Co^{2+}. These NO oxidation rates were consistent with the rates on Pt and PdO when one-electron-reduction processes, which were accessible for Rh^{4+} and Co^{3+} but not for Pt^{2+} and Pd^{2+}, were used to describe the reactivity of RhO_2 and Co_3O_4. One-electron redox cycles caused the $^{16}O_2$–$^{18}O_2$ exchange rates to be higher than the NO oxidation rates, in contrast with their analogous values on Pt and PdO, although O_2 activation on the vacancies limited NO oxidation and O_2 exchange on all of the catalysts. One-electron redox cycles allowed electron sharing between metal cations and a facile route to form vacancies on RhO_2 and Co_3O_4. This interpretation of the data highlighted the role of vacancies in kinetically relevant O_2-activation steps to explain the higher reactivity of larger metal and oxide clusters and to provide a common framework to describe NO oxidation and the active species on catalysts of practical interest.

Introduction

Nitrogen oxides must be removed from combustion exhaust to meet environmental regulations, which is particularly challenging for streams that contain O_2 and low concentrations of CO and hydrocarbons. Catalyst sites are titrated by strongly bound chemisorbed oxygen atoms (O*) during NO decomposition in the absence of reductants. As a result, open sites on O*-saturated surfaces, which are required for NO dissociation, are scarce.[1,2] Such conditions are unfavorable for NO conversion to N_2 and instead promote NO oxidation to NO_2. NO_2 is toxic but adsorbs on metal oxides[3–5] and reduces to N_2 when soot or hydrocarbons are present in exhaust streams.[6–9] These reactions provide an alternate abatement strategy for the removal of NO from lean-burn effluent streams, but require effective catalysts for NO oxidation into NO_2.

NO oxidation on Pt[10–12] and PdO[13] clusters involves kinetically relevant O_2 adsorption on vacant sites (*) at O*-saturated surfaces. The coverage of O* during NO oxidation is set by equilibrated NO–NO_2 interconversion.[11–13] The kinetic relevance of O_2 binding was confirmed by the identical rates of NO oxidation and the isotopic exchange of $^{16}O_2$–$^{18}O_2$.[12,13] These studies showed that NO oxidation rates decreased as the size of the metal or oxide cluster decreased because small clusters bound O* stronger than large clusters, thereby leading to lower vacancy concentrations on small clusters.

NO oxidation has also been catalyzed by Rh and Co clusters.[14–16] NO oxidation rates have been correlated with the reducibility of CoO_x clusters,[15] which suggested that O* binding and the availability of vacancies also determined the turnover

[a] Dr. B. M. Weiss, Dr. N. Artioli, Prof. E. Iglesia
Department of Chemical and Biomolecular Engineering
University of California, Berkeley
201 Gilman Hall, Berkeley, CA 94720 (USA)
Fax: (+1) 510-642-4778
E-mail: iglesia@berkeley.edu

[b] Prof. E. Iglesia
Chemical Sciences Division
E.O. Lawrence Berkeley National Laboratory
1 Cyclotron Rd., Berkeley, CA 94720 (USA)

[c] Dr. B. M. Weiss
Current Address:
ExxonMobil Research and Engineering
Annandale, NJ 08801 (USA)

[d] Dr. N. Artioli
Current Address:
Laboratory of Catalysis and Catalytic Processes
Energy Department
Politecnico di Milano 20133 Milano (Italy)

rates on Co catalysts. The rate data in previous studies were not attributed to specific elementary steps, which we do herein using kinetic and isotopic methods for both the RhO_2 and Co_3O_4 catalysts. NO oxidation on these catalysts involved similar elementary steps and site-requirements to those proposed on Pt and PdO. The turnover rates for NO oxidation and isotopic oxygen exchange were higher on Rh and Co oxides than on PdO and small Pt clusters and also than the rates that were expected from the energies of their metal–oxygen bonds. We attributed these results to the ability of RhO_2 and Co_3O_4 to undergo facile one-electron oxidation–reduction cycles during catalytic turnovers, which provided an alternate and more effective O_2-activation pathway than two-electron reduction on Pt and Pd catalysts.

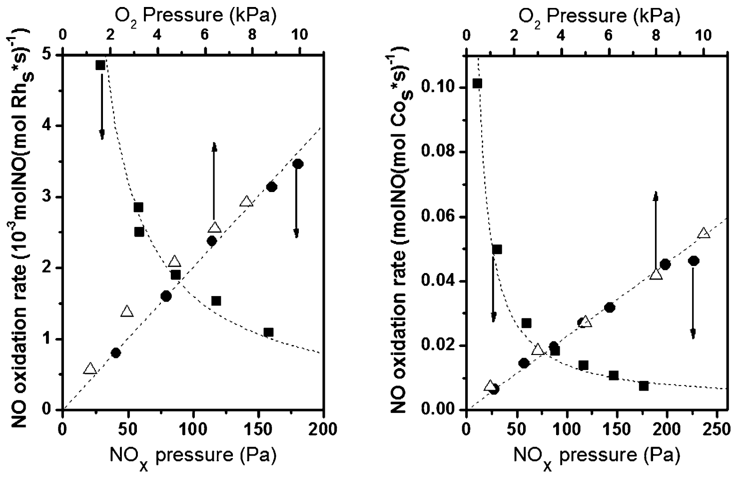

Figure 1. NO oxidation rates a) on 2.4 wt.% RhO_2/Al_2O_3 (573 K; H/Rh, 0.47) versus NO pressure (●; 0.055 kPa NO_2, 5 kPa O_2), NO_2 pressure (■; 0.11 kPa NO, 5 kPa O_2), and O_2 pressure (△; 0.11 kPa NO, 0.055 kPa NO_2); and b) on 10 wt.% Co_3O_4/SiO_2 (548 K; H/Co_r, 0.02) versus NO pressure (●; 0.060 kPa NO_2, 5 kPa O_2), NO_2 pressure (■; 0.12 kPa NO, 5 kPa O_2), and O_2 pressure (△; 0.12 kPa NO, 0.06 kPa NO_2).

Results and Discussion

NO oxidation kinetics on Rh and Co

NO oxidation rates were measured on Rh/Al_2O_3 and Co/SiO_2 as a function of the pressures of NO, NO_2, and O_2. The NO consumption rates reflected the dynamics of the forward ($\vec{r}_{NO}$) and reverse directions ($\overleftarrow{r}_{NO}$) of the stoichiometric chemical reaction, which corresponded to the rates of NO oxidation and NO_2 decomposition, respectively, according to Equation (1).

$$2\,NO + O_2 \rightleftharpoons 2\,NO_2 \quad (1)$$

The values of $\vec{r}_{NO}$ and $\overleftarrow{r}_{NO}$ are related by the approach-to-equilibrium factor (η)[17] according to Equation (2), where σ is a constant derived from the stoichiometric number and reaction affinity of each elementary step[18] and K_R is the equilibrium constant for Equation (1), as estimated from tabulated thermodynamic data.[18]

$$\eta = \frac{\overleftarrow{r}_{NO}}{\vec{r}_{NO}} = ([NO_2]^2[NO]^{-2}[O_2]^{-1}K_R^{-1})^{1/\sigma} \quad (2)$$

The forward NO oxidation turnover rates were obtained from the measured NO-conversion rates (r_{NO}) by using Equation (3).

$$r_{NO} = \vec{r}_{NO} - \overleftarrow{r}_{NO} = \vec{r}_{NO}(1-\eta) \quad (3)$$

Figure 1 shows the effect of the pressure of NO, NO_2, and O_2 on the forward NO oxidation turnover rates on Rh and Co catalysts. On all catalysts, the forward NO oxidation rates increased linearly with the pressure of NO and O_2 and were strongly inhibited by NO_2. The dashed lines in Figure 1 show that these data were consistent with Equation (4) and a value of η equal to one.

$$\vec{r}_{NO} = 2\,k_{NO}[O_2][NO][NO_2]^{-1} \quad (4)$$

This NO oxidation rate expression also described all rate data on Pt and PdO catalysts and was consistent with the elementary steps that were proposed previously for NO oxidation on these catalysts.[10–13] These steps involved kinetically relevant O_2 binding at unoccupied sites (*; Scheme 1 a) on the

$$O_2 + * \underset{}{\overset{k_1}{\rightleftharpoons}} O_2* \quad (a)$$
$$O_2* + * \overset{k_2}{\rightleftharpoons} 2O* \quad (b)$$
$$NO + O* \overset{K_3}{\rightleftharpoons} NO_2 + * \quad (c)$$

Scheme 1. Proposed elementary steps in NO oxidation.

cluster surfaces that were almost saturated with chemisorbed oxygen atoms (O*). Adsorbed O_2 molecules (O_2*) dissociated to form oxygen atoms (O*) in subsequent kinetically irrelevant steps (Scheme 1 b). The surface coverage of O* and * were set by quasi-equilibrated steps that involved the interconversion of NO and NO_2 on the cluster surfaces (Scheme 1 c). These steps, taken together with the steady-state approximation for all of the adsorbed species, led to a rate equation, shown in Equation (5)(), in which the denominator terms reflected the relative concentrations of * and O* during steady-state catalysis.

$$\vec{r}_{NO} = \frac{2k_1[O_2]}{1 + K_2[NO_2][NO]^{-1}} \quad (5)$$

This expression accurately described all kinetic data [Eq. (4)] when O* was the most-abundant surface intermediate [Eq. (6)].

$$\vec{r}_{NO} = \frac{2k_1}{K_2}\frac{[O_2][NO]}{[NO_2]} \quad (6)$$

Therefore, these rates indicated that the surfaces were almost saturated with O* and that the rate constant (k_{NO}) [Eq. (4)] was proportional to the ratio of k_1 and K_3.

The coverage of O* and the driving force for the formation of Rh and Co oxides depend on the oxygen chemical potential at the cluster surfaces. The oxygen chemical potential was determined by the virtual oxygen pressure (O_2^v) during NO oxidation catalysis.[12,13] O_2^v was established by NO–NO_2 adsorption equilibria, and the value of O_2^v was obtained by non-equilibrium thermodynamic treatment of chemical kinetics, according to Equation (7), in which K_R is the equilibrium constant for Equation (1), which could be calculated from tabulated thermodynamic data.[12,13]

$$[O_2^v] = [NO_2]^2[NO]^{-2}K_R^{-1} \tag{7}$$

O_2^v was the O_2 pressure that gave the same O* coverage at equilibrium as the O* coverage during steady-state NO oxidation catalysis at a given NO_2/NO ratio.

The equilibrium constant for NO_2 dissociation (K_3; Scheme 1 c) was related to the equilibrium constant for O_2 dissociation (K_O) by Equation (8).[12,13]

$$K_3 = K_O{}^{1/2}/K_R{}^{1/2} \tag{8}$$

The stoichiometry of step (c) corresponded to the difference between Equations (1) and (9).

$$O_2 + 2\,* \rightleftharpoons 2\,O* \tag{9}$$

The results in Equations (5), (7), and (8) showed that NO oxidation rates only depended on the O_2(g) pressure and on the prevailing oxygen chemical potential, which was given by O_2^v according to Equation (10).

$$\vec{r}_{NO} = 2k_1[O_2][*] = \frac{2k_1[O_2]}{1+(K_O[O_2^v])^{1/2}} \tag{10}$$

The assumption that O* was present at near saturation allowed a simplification of Equation (10). Thus, NO oxidation rates only depended on the O_2 pressure and on the chemical potential of oxygen at the working catalytic surfaces. Equation (11) was used to probe any residual dependence of the NO oxidation rate constants on O_2^v, which would indicate structural or composition changes that were associated with phase transitions, and to compare NO oxidation rates with $^{16}O_2$–$^{18}O_2$ exchange rates at similar O* coverage (see below).

$$\frac{\vec{r}_{O_2}}{[O_2]}\vec{r}_{NO} = k_1[*] = \frac{k_1}{(K_O[O_2^v])^{1/2}} \tag{11}$$

Oxidation state of Rh and Co during NO oxidation

The oxygen chemical potentials set by the NO/NO_2 reactions on the catalyst surfaces [Eq. (7)] represented the rigorous thermodynamic driving force for the prevalent O* coverage and also for oxide–metal phase-transitions during steady-state NO oxidation catalysis. Any changes in the measured NO oxidation rate constants with O_2^v [Eq. (7)] could reflect phase-transitions that were consequential to catalysis, whereas rate constants that did not depend on O_2^v preclude phase transitions that were consequential for catalysis within the experimental range of conditions. The rearrangement of Equation (11), shown in Equation (12), described all of the rate data, as shown by the linear dependence in Figure 2.

$$\left(\frac{[O_2]}{\vec{r}_{O_2}}\right)^2 = \frac{K_O}{k_1^2}[O_2^v] \tag{12}$$

The linear dependence showed that the NO oxidation rate constants on Rh and Co catalysts represented true constants that were unaffected by the oxygen chemical potentials (0.01–0.4 and 0.001–0.15 kPa O_2^v for Rh and Co, respectively) or by any metal–oxide transitions. We concluded that the oxidation state of the Rh- and Co clusters remained unchanged throughout this study and that they corresponded to the bulk phase, as dictated by these oxygen chemical potentials.

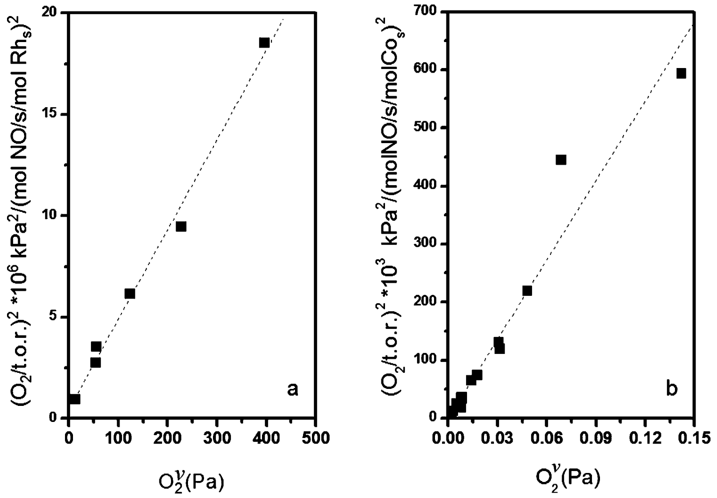

Figure 2. The ratio (O_2(g)/TOR)^2 plotted as a function of O_2^v [Eq. (7)] on a) RhO_2/Al_2O_3 (573 K; H/Rh, 0.47) and b) Co_3O_4/SiO_2 (548 K; H/Co_r, 0.02). The dashed line shows the regressed fit to [Eq. (11)]. The phase transitions for RhO_2/Rh_2O_3[20] at 573 K and for Co_3O_4/CoO[18] at 548 K occur at 3×10^{-2} and 7×10^{-15} Pa, respectively.

The phase diagram for bulk Rh oxides,[19] taken together with the thermodynamic data for bulk Rh, Rh_2O_3 ($\Delta H_f^{o} = -135$ kJ (mol O)$^{-1}$), and RhO_2 ($\Delta H_f^{o} = -122$ kJ mol^{-1})[20] and Co, CoO ($\Delta H_f^{o} = -237$ kJ (mol O)$^{-1}$), and Co_3O_4 ($\Delta H_f^{o} = -223$ kJ (mol O)$^{-1}$)[18] indicated that Rh and Co clusters existed as RhO_2 and Co_3O_4, respectively, under the conditions used herein (573–673 K, NO_2/NO 0.2–3.0, and 0.001–2 kPa O_2^v for Rh; 548–623 K, NO_2/NO 0.25–2, and 0.0001–2 kPa O_2^v for Co). Rh and Co form structures with lower metal oxidation states (Rh_2O_3 and CoO), but these oxides are only stable at significantly lower oxygen chemical potentials or at higher temperatures than used herein. For example, at 573 K, the RhO_2/Rh_2O_3 and Co_3O_4/CoO phase-transitions occurs at 10^{-6} and 10^{-14} kPa O_2, respectively. As a result, the predominant phases of each catalyst were Co_3O_4 or RhO_2 during steady-state catalytic NO oxidation for clusters of all sizes.

The oxidation state of Co during the catalysis was confirmed by O_2 uptake in the temperature range of NO oxidation catalysis. The O_2 uptake at 548 K on Co/SiO$_2$ (H/Co$_r$, 0.02) was 0.57 mol O_2 (mol Co)$^{-1}$ (O/Co, 1.14) after the sample had been pre-treated in H_2 at 673 K for 1 h and remained unchanged between 5 and 60 kPa O_2 (Figure 3). These data indicated that

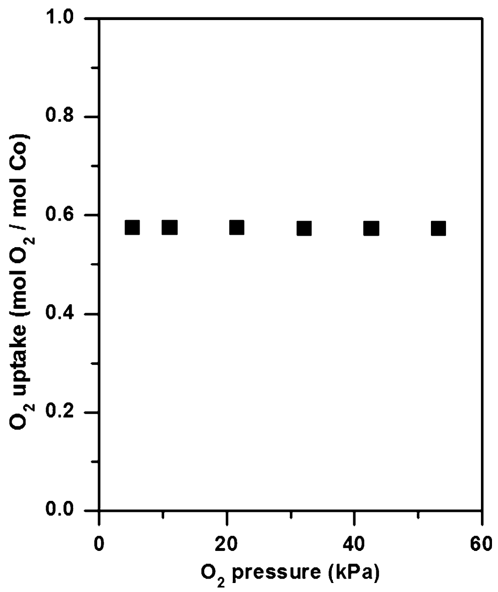

Figure 3. O_2 uptake at 548 K on 10 wt.% Co/SiO$_2$ (0.02 dispersion) that had been pre-treated at 673 K under a flow of 100 kPa H_2 for 1 h (0.1 cm^3 g^{-1} s^{-1}) and then under vacuum for 1 h.

most Co atoms (85%) were present as Co_3O_4 upon contact with O_2 and, therefore, with NO/NO$_2$ mixtures that provided equivalent oxygen chemical potentials during catalysis. The remaining Co atoms (15%) were present as Co silicates, which did not reduce during treatment in H_2 at 673 K[21–23] and therefore could not uptake O_2. The constant uptake with O_2 pressure (548 K, 5–60 kPa; Figure 3) showed that the clusters did not change their oxidation state over this pressure range, as expected from the thermodynamic data[18] and from the measured rate constants, which were independent of O_2^v (Figure 2 b).

Co^{3+} in Co_3O_4 and Rh^{4+} in RhO_2 could be reduced to Co^{2+} in CoO and Rh^{3+} in RhO_2, respectively, through one-electron reduction pathways. We inferred (see below) that the availability of these one-electron oxidation–reduction cycles influenced the pathways and dynamics of O_2 activation on RhO_2 and Co_3O_4 during both catalytic NO oxidation and $^{16}O_2$–$^{18}O_2$ isotopic exchange.

$^{16}O_2$–$^{18}O_2$ exchange and NO-oxidation rates

$^{16}O_2$–$^{18}O_2$ isotopic exchange and NO oxidation (Scheme 1 a) shared a common kinetically relevant step (O_2 adsorption on the vacant sites) on Pt and PdO clusters.[12,13] On Pt and PdO, these two reactions occurred at identical rates, irrespective of temperature or the oxygen chemical potential, which was consistent with their common limiting elementary step. Similar experiments were used herein to probe the kinetic relevance of O_2 activation during NO oxidation on RhO_2 and Co_3O_4 catalysts.

The O_2 activation rates ($r_{O_2(ex)}$) were determined from the measured $^{16}O_2$–$^{18}O_2$ isotopic exchange rates (r_{ex}) at 2 kPa O_2(g) in the absence of NO_x by using Equation (13), which describes the steady-state exchange rates, irrespective of the mechanism of exchange.[24]

$$r_{ex} = r_{O_2(ex)} \frac{[^{16}O_2][^{18}O_2]}{[O_2]^2}\left(1 - \frac{[^{16}O^{18}O]^2}{4[^{16}O_2][^{18}O_2]}\right) \tag{13}$$

In this equation, the terms in parenthesis account for the approach to isotopic equilibrium and the $[O_2]$ term denotes the sum of the pressures of all oxygen isotopologues ($[^{16}O_2]$,$[^{18}O_2]$, and $[^{16}O^{18}O]$). $\vec{r}_{O_2(ex)}$ is the O_2-activation rate, which depends on the total O_2 pressure and on the concentration of vacancies.[24]

Previous rate data on Co_3O_4 and other Group 8 metal oxides indicated that the O_2 exchange rates obeyed Equation (14), in which k_{ex} is the rate constant for O_2 activation.[24]

$$\frac{\vec{r}_{O_2(ex)}}{[O_2]} = k_{ex}[*] = \frac{k_{ex}}{\left(K_O[O_2]^{1/2}\right)} \tag{14}$$

Equation (14) was consistent with a rate-determining step for exchange that involved isolated vacancies on surfaces that were almost saturated with O*, as was also the case in NO oxidation [Eq. (11)]. The density of vacancies during exchange was given by the chemical equilibrium in Equation (9), with K_O as the equilibrium constant. Both Equation (14), which described O_2 exchange rates, and Equation (11), which described NO oxidation rates, probed O_2 activation rates on the clusters, which only depended on the rate constant for O_2 activation and on the availability of vacancies.

The rate constants of O_2 activation during exchange and during NO oxidation are shown in Figure 4. The NO-oxidation rate constants were measured at NO and NO_2 pressures that corresponded to O_2^v values of 2 kPa [Eq. (7)] and were compared with O_2-exchange rates that were measured at an actual total pressure of 2 kPa O_2(g). Figure 4 shows that k_{ex} [Eq. (13)] was larger than k_1 [Eq. (11)] by a factor of about 10 on Co_3O_4 and about 100 on RhO_2. The exchange rates were less affected by temperature than NO oxidation rates, thereby suggesting that oxygen exchange had a lower activation energy than NO oxidation. These results contrasted those reported on Pt and PdO clusters,[12,13] on which the NO oxidation rate constants were the same, within experimental accuracy.

The larger rate constants for exchange (k_{ex}) than for NO oxidation (k_1) on RhO_2 and Co_3O_4 (Figure 4) indicated that O_2 activation during $^{16}O_2$–$^{18}O_2$ exchange occurred by different elementary steps than those required for O_2 activation in NO–O_2 reactions. $^{18}O_2$ exchanged with lattice ^{16}O (^{16}O*) on some oxides[25,26] by a concerted three-atom transition state that mediates the O_2 activation and exchange elementary step

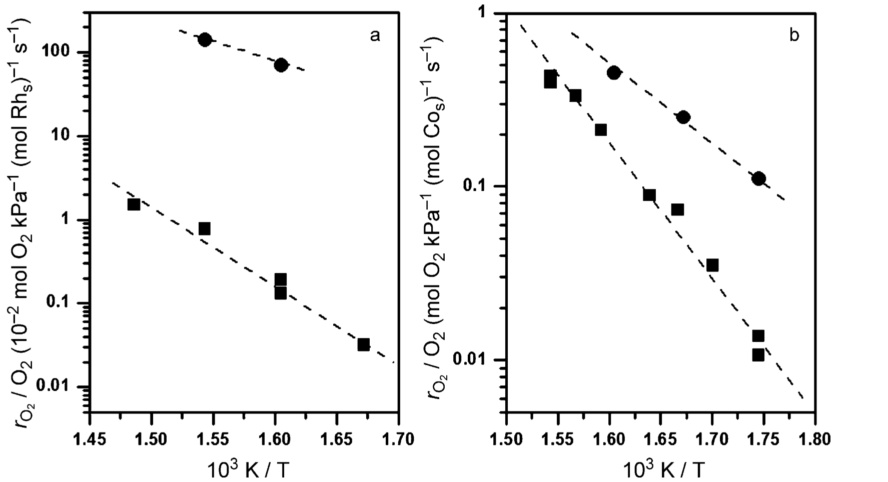

Figure 4. O_2 activation rates divided by the prevalent O_2 pressure during NO oxidation at 2 kPa O_2^v (■) and O_2 exchange at 2 kPa O_2 (●) on a) 2.4 wt.% Rh_2O_3/Al_2O_3 (0.47 dispersion) and b) 10 wt.% Co_3O_4/SiO_2 (0.01 dispersion).

NO oxidation, but not during isotopic exchange, which required only one electron transfer steps.

In spite of these differences in O_2 activation modes on Co_3O_4, RhO_2, Pt, and PdO, the kinetically relevant step for NO oxidation on all of the catalysts was the activation of O_2 on scarce vacancies at surfaces that were almost saturated with oxygen species. Such oxygen species were bound on Pt metal cluster surfaces or on exposed planes in bulk oxides of PdO, Co_3O_4, and RhO_2. The importance of oxygen vacancies in turnover rates suggests that NO oxidation turnover rates on all of the catalysts are sensitive to the oxygen chemical potential in the reacting mixture and to the strength of surface metal–oxygen bonds, which is discussed next.

(Scheme 2). This step does not lead to O_2 dissociation and, therefore, cannot contribute to NO oxidation turnovers, which require the ultimate dissociation of adsorbed O_2* into active O* species. These three-atom transition states are apparently formed much faster than O_2 dissociation transition states on RhO_2 and Co_3O_4, though both transition states involve the reaction of O_2 with vacant sites on the surfaces of clusters that are almost saturated with oxygen.

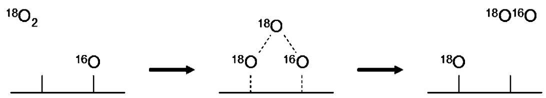

Scheme 2. Proposed mechanism of $^{16}O_2$–$^{18}O_2$ exchange on Co_3O_4 and RhO_2.

The rates of NO oxidation and O_2 exchange differed from each other on RhO_2 or Co_3O_4, but these two processes occurred at similar rates on Pt[12] or PdO.[13] This different behavior may reflect the ability of each catalyst to transfer electrons to adsorbed dioxygen molecules, as proposed previously for O_2 exchange.[25] Both Pd^{2+}[18] and Pt^{2+}[18] form Pd^0 or Pt^0 by direct two-electron reduction processes in aqueous electrochemical systems, but Co^{3+}[18] and Rh^{4+}[27,28] reduce sequentially by one-electron processes to give Co^{2+} and Rh^{3+}, respectively, as is also the case for such cations in their respective bulk oxides. Co^{3+} in Co_3O_4 and Rh^{4+} in RhO_2 undergo one-electron reductions to form Co^{2+} centers in CoO and Rh^{3+} in Rh_2O_3, whereas Pd^{2+} in PdO and Pt^{2+} in PtO and Pt_3O_4 reduce directly into their respective metals. From these differences between the Pt^{2+}/Pd^{2+} and Co^{3+}/Rh^{4+} reduction paths, we inferred that O_2 exchange proceeded by concerted reactions of O_2 with O* when metal centers at vacant sites undergo a one-electron reduction process. NO oxidation on Co_3O_4 and RhO_2 was slower than $^{16}O_2$–$^{18}O_2$ exchange, presumably because multiple electrons must be transferred to O_2 during the catalytic cycle for

Site requirements for NO oxidation on Rh- and Co oxides

The rates of NO oxidation on Rh and Co oxide clusters were normalized by the H_2 uptake on the reduced catalyst to account for the fraction of sites on the cluster surfaces. The rates of NO oxidation on dispersed RhO_2 clusters increased with increasing cluster size (Figure 5), which was consistent with the trends reported on Pt[10,12] and PdO[13] (Figure 5). The oxide clusters became more difficult to reduce with decreasing size, as their valence electrons became confined within smaller domains and their HOMO–LUMO gaps became larger.[29,30] Consequently, vacancies became more scarce as the oxide domains became less reducible with decreasing size, which caused NO oxidation turnover rates to decrease with decreasing size.

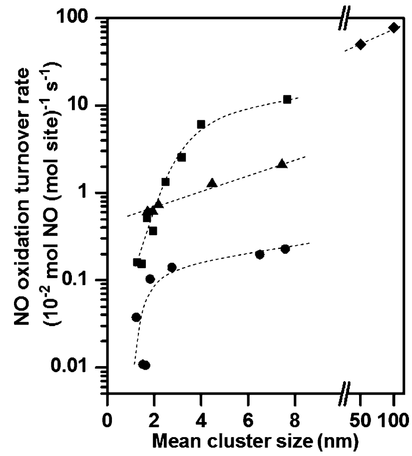

Figure 5. NO oxidation rates on RhO_2/Al_2O_3 (▲), Co_3O_4/Al_2O_3 (◆), Pt/Al_2O_3 (■),[12] and PdO/Al_2O_3[13] (●) at 603 K, 5 kPa O_2, 0.12 kPa NO, 0.056 kPa NO_2.

The turnover rates of NO oxidation on large Co_3O_4 clusters (40–100 nm) were much higher than those on all of the other catalysts examined (Figure 5). The NO oxidation rates on RhO_2 were higher than those on PdO and similar in magnitude to those on Pt clusters of similar size (Figure 4). The NO oxidation rate constant on each catalyst depended on the rate constant for O_2 activation (k_1) and on the O* binding energy (K_3 or K_O; [Eq. (6)] or [Eq. (11)]). The O*-binding energies accounted for the cluster-size effects on NO oxidation (Figure 5); thus, they must also account for the trends in NO oxidation rates among these different catalytic elements.

Indeed, Pd(111) binds O* more strongly than Pt(111) by about 30 kJ mol^{-1}.[31] This difference in O* binding energies apparently persisted on working catalysts (PdO and Pt surfaces that were saturated with O*), which was consistent with the lower NO oxidation rates on the PdO catalysts (Figure 5). However, in their metallic states, Rh(111) and Co(111) bind O* much more strongly than Pt(111) or Pd(111) by 100–200 kJ mol^{-1}.[31] Yet, the NO-oxidation turnover rates on Rh and Co oxides were much higher than on Pt or PdO and higher than expected from the high O*-binding energies on the Rh and Co metals (Figure 5). Clearly, the O*-binding energies on the Rh and Co metal surfaces were not accurate descriptors of reactivity because they were not inherently relevant to the stability and concentration of vacancies on catalysts that existed as oxides during NO oxidation catalysis.

The formation of vacancies on clusters that were almost saturated with oxygen occurs by the formal reduction of cations that were bound to chemisorbed or lattice oxygen atoms. The thermodynamics of such events should parallel those of electrochemical redox cycles. The standard reduction potential for Co^{3+}/Co^{2+} cycles (1.8 V) are significantly larger than for Pt^{2+}/Pt^0 cycles (1.3 V), which, in turn, are larger than for Pd^{2+}/Pd^0 cycles (0.9 V)[18] (Figure 6). These reduction potentials indicated that the reduction of Co^{3+} into Co^{2+} was more facile than the reduction of either Pt^{2+} or Pd^{2+} to their corresponding zero-valent states. For these systems, the turnover rates and electrochemical reduction potentials for NO oxidation appeared to share common features that caused the correlation evident for Co_3O_4, Pt, and PdO (Figure 6). The correlation in Figure 6 suggested that the thermodynamics of the electrochemical redox cycles paralleled the thermodynamics of vacancy formation on the catalyst surfaces, which, in turn, affected O_2 adsorption rates at a given oxygen chemical potential during NO oxidation. The wide range of reduction potentials that have been reported for the Rh^{4+}/Rh^{3+} reduction cycles (0.8–1.7 V for different coordinating ligands)[27,28] made correlation with the reactivity of NO oxidation less precise than for other metal systems, but the reported reduction potentials and the rates of NO oxidation on Rh^{4+} also followed the trend in Figure 6. NO oxidation rate data suggested that the reduction tendency (and vacancy density) of RhO_2 clusters lay between that for Pt and PdO and was much greater than that indicated by the reduction potential for the Rh^{3+}/Rh^0 cycles (Figure 6).

The correlation between NO oxidation rates and redox potentials (Figure 6) suggested that the high NO oxidation turnover rates on RhO_2 and Co_3O_4 reflected the ability of Rh^{4+} and Co^{3+} to undergo one-electron reductions, which were more facile than reductions that required the transfer of two electrons from a single cationic center. Such facile one-electron transitions in RhO_2 and Co_3O_4 led to higher vacancy concentrations on these substrates than expected from the redox potentials for the Rh^{3+}/Rh^0 and Co^{2+}/Co^0 transitions (Figure 6) and from the strong binding of O* on Rh and Co metals. Moreover, the higher rates of $^{16}O_2$–$^{18}O_2$ exchange than NO oxidation on RhO_2 and Co_3O_4 also appeared to reflect the ability of these substrates to undergo one-electron redox cycles. The effects of the one-electron cycles on NO oxidation rates (Figure 6) and the much higher rates for $^{16}O_2$–$^{18}O_2$ exchange than for NO oxidation on RhO_2 and Co_3O_4 (but not on Pt or PdO; Figure 4) indicated that O_2 dissociation to form O* atoms during NO oxidation involved multiple Co^{3+} or Rh^{4+} centers, whereas O_2 activation during $^{16}O_2$–$^{18}O_2$ exchange by the steps in Scheme 2 only occurred on one Co^{3+} or Rh^{4+} center.

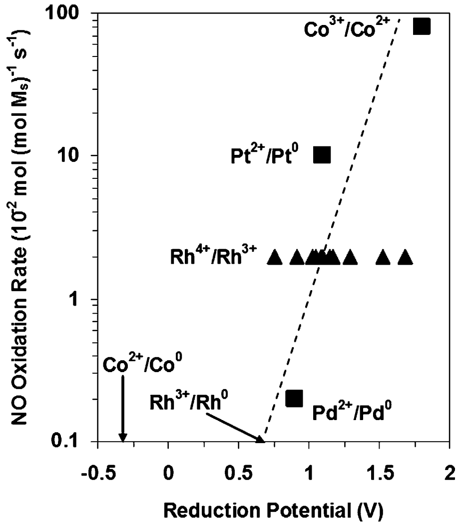

Figure 6. (■) NO oxidation rates on Co_3O_4 (50 nm), Pt (8 nm[12]), and PdO (8 nm[13]) at 603 K, 5 kPa O_2, 0.12 kPa NO, 0.056 kPa NO_2 versus the reduction potential of the corresponding aqueous cation (298 K, 1 M, 20 kPa O_2[18]). Arrows show the reduction potentials for Co^{2+}/Co^0 and Rh^{3+}/Rh^0.[18] (▲) NO-oxidation rates on RhO_2 (8 nm) versus the reduction potential of Rh^{4+}/Rh^{3+}. The values for Rh^{4+}/Rh^{3+} reflect the effects of coordinating ligands on the redox properties.[27,28]

Co oxides have been reported to exhibit high reactivity for the electrochemical conversion of H_2O into O_2, a reaction that shares elementary steps with NO oxidation[32,33], because both require oxygen vacancies in their respective kinetically relevant steps. In the conversion of H_2O, vacancies form by the reduction of Co^{4+} into Co^{3+},[32,33] apparently through similar one-electron transitions that occurred on Co^{3+} during NO oxidation.

These mechanistic connections between the thermodynamics of electrochemical reduction and NO oxidation turnover rates (Figure 6) indicated a fundamental resemblance between the electron-transfer processes in solvated coordination complexes and inorganic oxides. For both, their reduction tendencies reflected the energy levels of the frontier orbitals that accepted electrons, which were set by metal–ligand and electron–electron interactions. Theoretical estimates of such energies remain uncertain, because DFT methods do not yet accurately describe the critical electron–electron interactions that influenced the thermodynamics of the electron-transfer processes in inorganic solid oxides.[34] The connections inferred herein between the reduction tendencies of aqueous metal complexes and solid oxides (and their consequences for reduction–oxidation catalysis) provide significant impetus for parallel efforts in the development and use of more exact theoretical approaches to describe the redox properties of solids, if so required by the use of coordination complexes as model systems that are more amenable to rigorous theoretical treatments to assess the accuracy of these theoretical methods.

Conclusions

The effect of the pressures of NO, NO_2, and O_2 on NO oxidation rates on RhO_2 and Co_3O_4 were consistent with a mechanism in which O_2 binding on oxygen atom vacancies was the kinetically relevant step for NO oxidation; the same mechanism was also observed on Pt and PdO. Equilibrated reactions that involved NO and NO_2 established the vacancy concentrations and oxygen chemical potentials at the catalyst surfaces. The chemical potentials of oxygen that was prevalent during NO oxidation caused Rh and Co clusters to exist as RhO_2 and Co_3O_4 during catalysis. The prevalence of RhO_2 and Co_3O_4 had several consequences for NO oxidation and O_2 activation on the catalyst surfaces: NO-oxidation rates increased with increasing cluster size because small oxide and metal clusters bound oxygen more strongly than large clusters, thereby resulting in lower concentrations of vacant sites that bind O_2 in kinetically relevant steps and lower NO oxidation rates. Both RhO_2 and Co_3O_4 had cations (Rh^{4+} and Co^{3+}) that reduced by one-electron redox cycles to form vacancies, which led to higher rates of $^{16}O_2$–$^{18}O_2$ exchange on RhO_2 and Co_3O_4 than NO oxidation because exchange occurred by an O_2 activation pathway that only required a one-electron transfer, whereas NO oxidation required O_2 dissociation to oxygen atoms by slower and consecutive one-electron reductions of Co^{3+} or Rh^{4+} in Co_3O_4 or RhO_2. NO oxidation rates on all of the catalysts correlated to the electrochemical redox potential when the one-electron transitions that involved Co^{3+}/Co^{2+} and Rh^{4+}/Rh^{3+} were used to describe the reducibility of Co_3O_4 and RhO_2. The presence of the one-electron pathways on Co_3O_4 and RhO_2 led to NO-oxidation rates that were higher than expected from the large O*-binding energy on Rh and Co metal, thereby causing both to be effective as catalysts for NO oxidation.

Experimental Section

Catalyst synthesis and characterization

γ-Al_2O_3 (Sasol, SBa-200, 180 m^2g^{-1}) and SiO_2 (Davisil, Grade 646, 300 m^2g^{-1}) supports were heated to 1023 K at 0.07 Ks^{-1} under a flow of dry air (Praxair, Extra Dry, 1 $cm^3s^{-1}g^{-1}$) and held at 1023 K for 4 h. $[Rh(NO_3)_3]\cdot H_2O$ (Sigma–Aldrich) or $[Co(NO_3)_2]\cdot(H_2O)_6$ (Sigma–Aldrich) were added to deionized distilled water (Barnstead, Nanopure) and the solution was added dropwise to γ-Al_2O_3 or SiO_2 until the incipient wetness point was reached [0.45 g solution (γ-Al_2O_3)$^{-1}$, 0.9 g solution (g SiO_2)$^{-1}$] to give samples with 0.8% and 2.4 wt.% Rh and 10 wt.% Co. The impregnated supports were heated in air at 393 K for 4 h and then in a flow of dry air (Praxair, extra dry, 1 $cm^3s^{-1}g^{-1}$) for 4 h at 0.07 Ks^{-1} to a temperature between 673–1148 K. Rh- or Co-containing samples were then heated to 873 K or 673 K at 0.07 Ks^{-1}, respectively, and held at that temperature in 9% H_2/He (Praxair, 99.999% purity, 1 $cm^3s^{-1}g^{-1}$) for 5 h. The materials were treated with 0.5% O_2/He (Praxair, 99.999% purity, 1 $cm^3s^{-1}g^{-1}$) at 295 K for 1 h before exposure to ambient air.

H_2 and O_2 uptakes were measured volumetrically (Autosorb-1; Quantachrome) to determine the number of Rh and Co atoms that were exposed at the cluster surfaces (Rh_s and Co_s) and the number of reducible Co atoms (Co_r). The samples (0.5–1.0 g) were heated to 673 K at 0.08 Ks^{-1} and held at 673 K for 2 h under a flow of H_2 (1 bar) and then evacuated for 1 h at 673 K before the H_2- or O_2-uptake measurements were recorded at 313 K and 673 K, respectively, and at 5–50 kPa titrant pressure. The uptake isotherms were extrapolated to zero pressure to exclude any contributions from weakly bound species. The mean cluster diameters were estimated from measured uptakes by using the assumption of one chemisorbed H atom per surface Rh or Co atom (denoted Rh_s or Co_s), 1.33 O atoms per reducible Co atom, and hemispherical clusters with densities of bulk Rh or Co (Rh: 12.4 $g\,cm^{-3}$, 72 nm^{-3}; Co: 8.9 $g\,cm^{-3}$, 91 nm^{-3}).[18]

NO oxidation rate measurements

NO oxidation rates were measured on 0.12–0.18 mm Rh/Al_2O_3 and Co/SiO_2 aggregates. The samples were held on a porous quartz frit within a tubular quartz reactor (10 mm). The reactants (15% O_2/He, 2% NO/He, and 1% NO_2/He) and He carrier (Praxair, 99.999% purity) were metered by using electronic controllers (Porter Instruments) to achieve a broad range of reactant pressures (1–12 kPa O_2, 0.04–0.25 kPa NO, and 0.02–0.25 kPa NO_2). A resistively heated furnace with a controller (Watlow, 96 series) and a K-type thermocouple was used to maintain a constant temperature (548–673 K). The inlet and outlet concentrations were measured by using an infrared analyzer (MKS 2030; 2 cm^3 cell; 2 cm pathlength; 338 K). NO oxidation rates are reported as turnover rates [TOR, mol NO converted (mol Rh_s or Co_s)$^{-1}$ s^{-1}] at NO conversions below 15%. Heat and mass transfer artifacts were ruled out by previous experiments under similar conditions.[12]

Isotopic oxygen exchange measurements

$^{16}O_2$–$^{18}O_2$-exchange rates were measured by using a gradient-less batch reactor (volume: 498 cm^3) in which the reactants were circulated by a graphite gear pump (Micropump; 2 cm^3s^{-1}). The gases (99.999% chemical purity) were obtained from Praxair (90% O_2/Ar, He) and Ikon Isotopes ($^{18}O_2$, 96% isotopic ^{18}O purity). The catalysts were heated to 573–653 K at 0.07 Ks^{-1} and held at that temperature for 1 h under a flow of 2 kPa $^{16}O_2$/Ar/He (30 $cm^3s^{-1}g^{-1}$) before the reactor was evacuated and filled with an equimolar $^{16}O_2$-$^{18}O_2$ mixture and He as a balance. The isotopologue concentrations were measured by the periodic injection of pulses into a mass spectrometer (MKS Mini-Lab).

Acknowledgements

We are grateful for financial support from The Ford Motor Company, General Motors, the Chevron Corporation, and the Chemical Sciences, Geosciences, and Biosciences Division, Office of Basic Energy Sciences, Office of Science, US Department of Energy (grant no. DE-FG02-03ER15479).

Keywords: cobalt · gas storage · oxidation · oxygen · rhodium

[1] A. Amirnazmi, M. Boudart, *J. Catal.* **1973**, *30*, 55.
[2] A. Amirnazmi, M. Boudart, *J. Catal.* **1975**, *39*, 383.
[3] N. Takahashi, H. Shinjoh, T. Iijima, T. Suzuki, K. Yamazaki, K. Yokota, H. Suzuki, N. Miyoshi, S. Matsumoto, T. Tanizawa, T. Tanaka, S. Tateishi, K. Kasahara, *Catal. Today* **1996**, *27*, 63.
[4] N. W. Cant, M. J. Patterson, *Catal. Today* **2002**, *73*, 271.
[5] S. Roy, A. Baiker, *Chem. Rev.* **2009**, *109*, 4054.
[6] A. Kato, S. Matsuda, T. Kamo, F. Nakajima, H. Kuroda, T. Narita, *J. Phys. Chem.* **1981**, *85*, 4099.
[7] M. Koebel, M. Elsener, G. Madia, *Ind. Eng. Chem. Res.* **2001**, *40*, 52.
[8] B. R. Stanmore, J. F. Brilhac, P. Gilot, *Carbon* **2001**, *39*, 2247.
[9] F. Jacquot, V. Logie, J. F. Brilhac, P. Gilot, *Carbon* **2002**, *40*, 335.
[10] S. S. Mulla, N. Chen, L. Cumaranatunge, G. E. Blau, D. Y. Zemlyanov, W. N. Delgass, W. S. Epling, F. H. Ribeiro, *J. Catal.* **2006**, *241*, 389.
[11] S. S. Mulla, N. Chen, W. N. Delgass, W. S. Epling, F. H. Ribeiro, *Catal. Lett.* **2005**, *100*, 267.
[12] B. M. Weiss, E. Iglesia, *J. Phys. Chem. C* **2009**, *113*, 13331.
[13] B. M. Weiss, E. Iglesia, *J. Catal.* **2010**, *272*, 74.
[14] A. Amberntsson, E. Fridell, M. Skoglundh, *Appl. Catal. B* **2003**, *46*, 429.
[15] M. M. Yung, E. M. Holmgreen, U. S. Ozkan, *J. Catal.* **2007**, *247*, 356.
[16] D. S. Kim, Y. H. Kim, J. E. Yie, E. D. Park, *Korean J. Chem. Eng.* **2010**, *27*, 49.
[17] W. L. Holstein, M. Boudart, *J. Phys. Chem. B* **1997**, *101*, 9991.
[18] W. M. Haynes, CRC Press/Taylor and Francis, Boca Raton, FL, **2011**.
[19] O. Muller, R. Roy, *J. Less-Common Met.* **1968**, *16*, 129.
[20] K. T. Jacob, D. Prusty, *J. Alloys Compd.* **2010**, *507*, L17.
[21] S. L. Soled, E. Iglesia, R. A. Fiato, J. E. Baumgartner, H. Vroman, *Top. Catal.* **2003**, *26*, 101.
[22] G. Jacobs, T. K. Das, Y. Zhang, J. Li, G. Racoillet, B. H. Davis, *Appl. Catal. A* **2002**, *233*, 263.
[23] A. Martinez, C. Lopez, F. Marquez, I. Diaz, *J. Catal.* **2003**, *220*, 486.
[24] G. Boreskov, *Adv. Catal.* **1965**, *15*, 285.
[25] E. R. S. Winter, *J. Chem. Soc. A* **1968**, 2889.
[26] C. Doornkamp, M. Clement, V. Ponec, *J. Catal.* **1999**, *182*, 390.
[27] C. Guharoy, R. J. Butcher, S. Bhattacharya, *J. Organomet. Chem.* **2008**, *693*, 3923.
[28] M. Maestri, D. Sandrini, V. Balzani, U. Maeder, A. Von Zelewsky, *Inorg. Chem.* **1987**, *26*, 1323.
[29] L. Brus, *J. Chem. Phys.* **1984**, *80*, 4403.
[30] Y. Wang, N. Herron, *J. Phys. Chem.* **1991**, *95*, 525.
[31] R. A. van Santen, M. N. Neurock, *Molecular Heterogeneous Catalysis: A Conceptual and Computational Approach*, Wiley, Hoboken, NJ, **2006**.
[32] J. B. Gerken, J. G. McAlpin, J. Y. C. Chen, M. L. Rigsby, W. H. Casey, R. D. Britt, S. S. Stahl, *J. Am. Chem. Soc.* **2011**, *133*, 14431.
[33] Y. Surendranath, M. W. Kanan, D. G. Nocera, *J. Am. Chem. Soc.* **2010**, *132*, 16501.
[34] A. T. Bell, M. Head-Gordon, *Annu. Rev. Chem. Biomol. Eng.* **2011**, *2*, 453.

Received: January 29, 2012
Published online on ■■ ■■, 0000

NO catalyst is an island: The oxidation of NO on RhO_2 and Co_3O_4 is limited by the activation of O_2 at vacancies on oxygen-saturated surfaces. Oxygen-binding energies set the vacancy densities and turnover rates. One-electron reductions that are accessible to RhO_2 and Co_3O_4 facilitate O_2 activation and allow faster $^{16}O_2$–$^{18}O_2$ exchange and NO oxidation than expected from their oxygen-binding strengths.

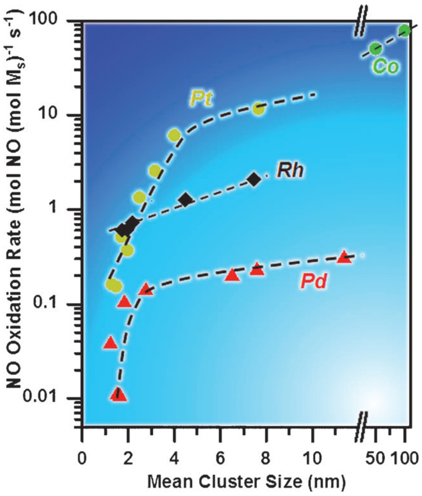

B. M. Weiss, N. Artioli, E. Iglesia*

■■–■■

Catalytic NO Oxidation Pathways and Redox Cycles on Dispersed Oxides of Rhodium and Cobalt

